Eur. Phys. J. A **30**, 461–467 (2006)
DOI 10.1140/epja/i2006-10130-9

THE EUROPEAN PHYSICAL JOURNAL A

A microscope for the Glasgow photon tagging spectrometer in Mainz

A. Reiter[2,a], P.S. Lumsden[1], J. Ahrens[2], J.R.M. Annand[1], R. Beck[2,b], J.C. McGeorge[1,c], and R.O. Owens[1]

[1] Department of Physics and Astronomy, University of Glasgow, Glasgow G12 8QQ, Scotland, UK
[2] Institut für Kernphysik, Universität Mainz, D-55099 Mainz, Germany

Received: 27 July 2006 / Revised: 12 September 2006 /
Published online: 3 November 2006 –
Communicated by Th. Walcher

Abstract. A 96-element plastic-scintillator detector array has been constructed to improve the energy resolution and tagged-photon flux over a moveable energy range of up to 60 MeV in the Glasgow photon tagging spectrometer at Mainz. Test results are presented which demonstrate that this device improves the resolution by a factor of about 6 compared to the main detector array. It is also shown that it is possible to achieve accurate energy calibration by using electron beams of several different accurately known energies from the Mainz accelerator.

PACS. 29.40.Mc Scintillation detectors – 29.30.Dn Electron spectroscopy

1 Introduction

With the advent of high duty-cycle electron accelerators, Bremsstrahlung photon tagging has become the technique of choice in most experiments where a high-intensity photon beam of known energy is required, and tagging spectrometers [1–3] have been installed at several laboratories. The Glasgow photon tagging spectrometer [4,5] installed at the Mainz 883 MeV electron microtron, MAMI [6–8], has been used successfully in many photonuclear experiments. The tagged energy range is $\sim$ 41–818 MeV and, although the intrinsic resolution of the spectrometer dipole magnet is $\sim$ 0.15 MeV, in practice the energy resolution ($\sim$ 2 MeV) is set by the widths of the 353 scintillators in the focal-plane detector. These detectors also limit the useful tagged-photon intensity to about 5×10^5/MeV·s due to background from random coincidences and to the long-term need to limit wear in the photomultiplier tubes and radiation damage in the scintillators. At the maximum tagged-photon intensity the dead time in the focal-plane detectors is $< 4\%$ and the anode current in the photomultiplier tubes is well below that at which the gain changes significantly.

Both the resolution and the maximum useful intensity can be improved, in principle, by increasing the segmentation of the focal-plane detector. With this in mind, the main detector array was not positioned in the focal plane, but displaced outwards from the magnet to leave a $\sim$ 50 mm gap (see fig. 1), so that a detector of higher segmentation may be inserted in the focal plane over most of the tagged energy range.

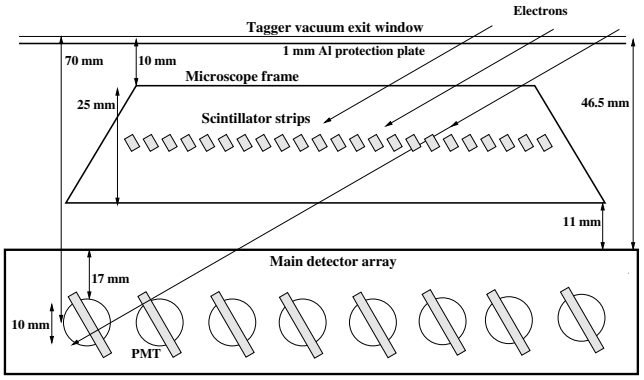

Fig. 1. Location (schematic) of the tagger microscope and main detector array.

In many experiments, the $\sim$ 2 MeV energy resolution provided by the main detector array is sufficient, but in some experiments better resolution would be valuable, at least over a small part of the tagged energy range. This can sometimes be the case in experiments with linearly polarised photons produced by a diamond radiator because the degree of polarisation is only high over a narrow photon energy range [9–12]. Detailed measurements of photoreaction cross-sections in the threshold region also

[a] *Present address:* Gesellschaft für Schwerionenforschung mbH, Planckstrasse 1, 64291 Darmstadt, Germany.
[b] *Present address:* University of Bonn, Germany.
[c] e-mail: j.mcgeorge@physics.gla.ac.uk

fall into this category. For example, the measurement [13] of the η photoproduction cross-section which gave a measurement of the η mass could be improved with better resolution, but this is only necessary in the region near the η threshold. In general, for such experiments it is useful to cover a region of about 20 MeV below threshold in order to confirm that backgrounds are under control, while a region of about 30 MeV above threshold is sufficient to determine the energy dependence of the cross-section in the threshold region.

The 96-element detector array (tagger microscope) described here offers improved resolution by factors in the range 2 to 6, and increased tagged flux by a factor of ~ 2. For an electron beam energy of 883 MeV this array spans an energy range of ~ 60 MeV and it may be positioned as required to select the tagged-photon energies of interest.

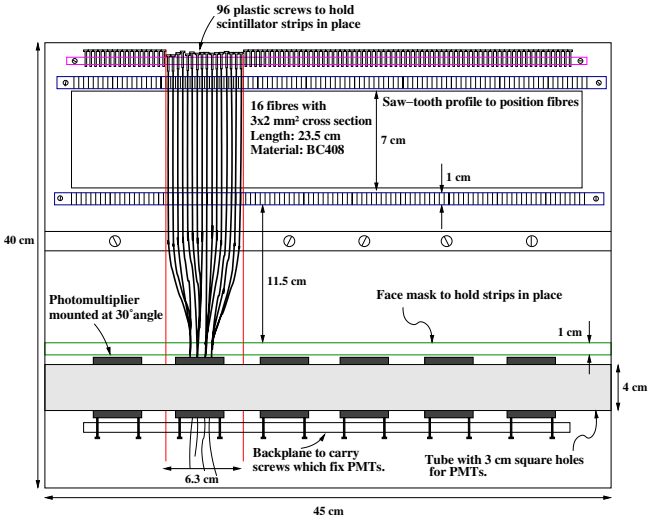

Fig. 2. Schematic drawing of the tagger microscope.

2 The microscope

Higher segmentation obviously implies smaller detectors. The scintillators in the main detector array (fig. 1) are half overlapping, about 13 mm wide on average and coincident neighbouring hits are required in the hardware (see [5]) so that a "channel" is effectively about 6.5 mm wide. To achieve an improvement in resolution by a factor of > 5 therefore requires an effective detector width of < 1.3 mm, and to cover 50 MeV requires about 150 detector channels.

Although other detector types were considered, scintillation counters were chosen because they are simple, fast, fairly resistant to radiation damage and have relatively low cost.

Some initial tests were made using $2 \times 2 \times 200$ mm pairs of clad scintillating fibers (BCF10). These fibers have the advantage of a long attenuation length (> 1 m) and they are mechanically flexible, but their light capture fraction (for light transport along the fibre by internal reflection) is rather low ($\sim 3\%$). One problem with any close-packed scintillator array is finding space for the photomultiplier tubes. This problem was solved by using multianode photomultiplier tubes (Hamamatsu 6568) where the cathode is divided into 16 4×4 mm pixels. In tests with the clad scintillating fibres it was found that the signals produced by the relativistic tagging electrons were so small (only a few photoelectrons at the cathode of the photomultiplier tube) that a significant fraction fell below the discriminator level needed to suppress noise in the photomultiplier tubes. Also the cladding (thickness about 4% of the total) gives rise to small dead regions so that some tagging electrons go undetected.

Tests with a collimated Sr90 source showed that the signals were a factor of about 5 larger from $3 \times 2 \times 235$ mm strips of plastic scintillator (BC408) individually wrapped in aluminised mylar, although part of this improvement could have been due to improved optical coupling between the scintillator and the photomultiplier tube. Because the cross-section is substantially smaller than the 4×4 mm pixel area on the photomultiplier tubes, cross talk is small even if neighbouring detectors are connected to neighbouring pixels. This in turn eases mechanical construction as only modest bending of the scintillator strips is necessary to adapt the in-line positioning at the focal plane to the 4×4 geometry at the photomultiplier tube. This was easily achieved with a heat gun at a temperature of about 70 °C and therefore it was decided to construct a device with these scintillator strips. By mounting the strips one third overlapping an effective 1 mm channel width was achieved by identifying single hits and neighbouring double hits. The only disadvantage of this arrangement is that the widths of neighbouring channels become unequal when the tagging electrons are not normally incident on the 3 mm face (see fig. 6 and sect. 3).

The schematic layout of the device and details of the support frame are shown in fig. 2. Two bars containing machined "sawtooth" apertures and separated vertically by 90 mm hold the scintillator strips parallel to and one third overlapping each other (fig. 1). The frame also holds the strips at the correct angle (30°) to the focal plane so that, in the middle of the energy range covered by the spectrometer, the tagging electrons enter normal to the 3 mm strip face. Away from the central region, the angle of the tagging electron trajectories with respect to the focal plane varies between about 20° and 40° so that over the full tagged range the incident angle differs from normal by up to about 10°. This results in unequal single- and double-hit channel widths (see sect. 3).

At the photomultiplier end the scintillator strips pass through spark eroded rectangular holes in an aluminium block (fig. 2) which aligns them to the pixels of the multianode photomultiplier tubes. Optical coupling compound (Dow Corning DC Q2-3067) between the ends of the scintillator strips and the photomultiplier tubes was used to improve transmission to the photocathode and a plastic screw bearing on the far end of every strip (see fig. 2) was adjusted to obtain and maintain good optical contact.

The scintillator strips themselves extend all the way to the photomultiplier tube window to avoid a joint between the scintillator and a passive light guide which would be a potential source of mechanical instability and signal losses.

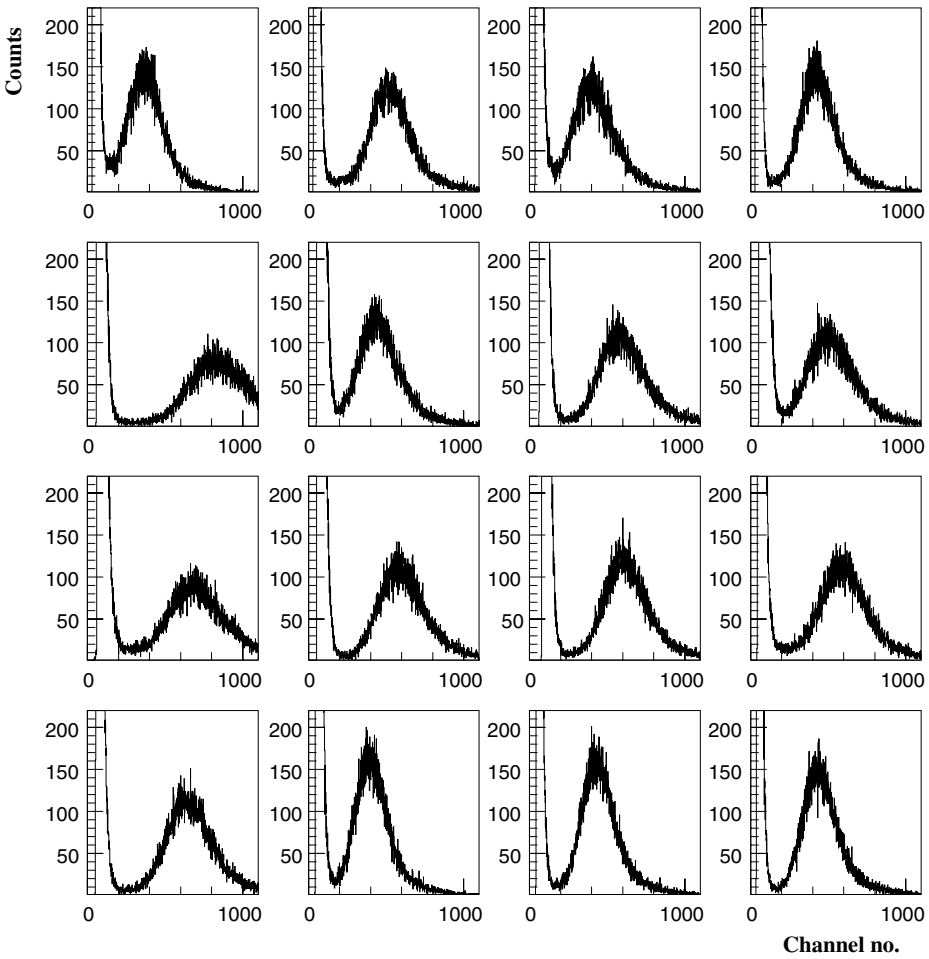

Fig. 3. Typical pulse height spectra from the microscope elements. These spectra were taken with the microscope in the middle of the focal plane where the incident tagging electron trajectory is normal to the face of the scintillators. Each photomultiplier pixel has a different gain which is not adjustable individually.

This results in a greater sensitivity to room background, but it was found to be negligible except for the "single-hit" channels at very low beam intensity (such as may be used in "tagging efficiency" measurement —see [5]). In this case the background can be easily measured and subtracted.

The more recent version of the H6568 multi-anode photomultiplier tube with thinner (0.8 mm) entrance window was installed as this is thought to be less prone to "cross talk" between different pixels. The Hamamatsu base chain where the dynode potentials are actively stabilised was specified in order to improve the gain stability at high counting rates.

The 96 scintillator strips and 6 photomultiplier tubes are mounted on a compact frame (fig. 2) which can be inserted at any location along the tagger focal plane corresponding to photon energies between 150 and 735 MeV. At higher photon energy access is restricted by the outer return yoke of the spectrometer [4].

The signals from the photomultiplier tubes were amplified by a factor of 10 (Phillips 7176) and fed to LeCroy 1885 charge-to-digital convertors (QDCs) for gain monitoring, and, via CAEN CF208 constant fraction discriminators (CFDs), to scalers (Struck STR 200) and the stop inputs of LeCroy 1875 time-to-digital convertors (TDCs). The TDC start signal is normally provided by the main experiment trigger detector which is fired by some reaction product produced by the tagged photons, but may also be provided by an OR of the microscope signals for calibration and testing.

3 Tests of microscope performance

The performance of the microscope has been assessed from tests carried out with it inserted at several places in the focal plane of the spectrometer. The pulse height response of some of the strips to the minimum ionising tagging electrons is shown in fig. 3. It can be seen that the pulse height distribution, resulting from a Landau energy loss distribution folded with the detector resolution, is well separated from the photomultiplier tube noise. Discriminator thresholds can therefore be set to reject noise, with negligible loss of tagging electrons. Typical losses below threshold are about 2%. The gain was found to be stable up to a tagged-photon flux of about $10^6/\mathrm{MeV}\cdot\mathrm{s}$ (where the count

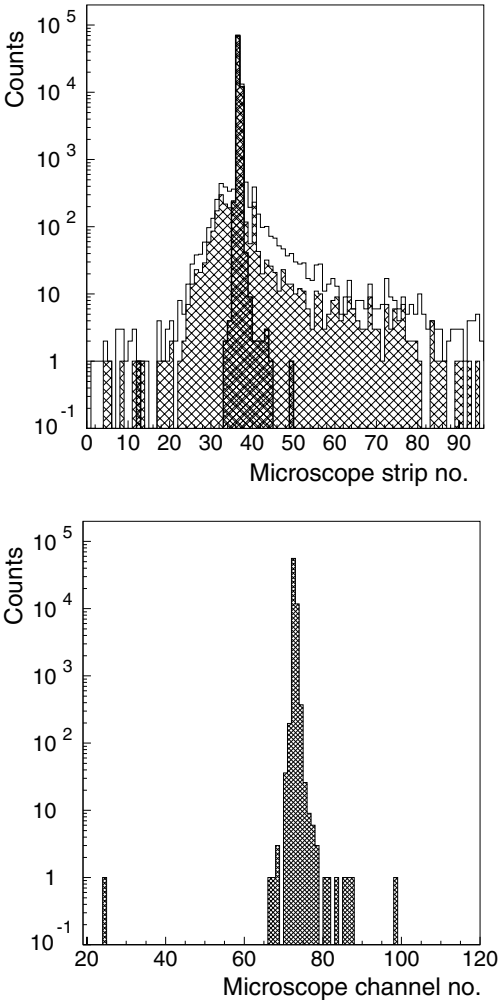

Fig. 4. Typical microscope response to a 180.1 MeV calibration electron beam with a field of 1.08 T in the spectrometer. The microscope was positioned to cover the tagged-photon energy range from 673 to 728 MeV for an incident 883 MeV electron beam which uses the same field. The upper plot shows the counts in the strips. The thin-line histogram shows the spectrum with no conditions. In the medium-hatched histogram events with strip multiplicity greater than 2 are rejected. In the densely hatched histogram events with non-adjacent double hits are also rejected. The lower plot shows the "channels" (see text) spectrum subject to the latter condition.

rate per pixel in the photomultiplier tube is about 10^6/s) above which it decreases. A useful fraction of the electrons are counted up to a rate of about $1.5 \times 10^6/\text{MeV} \cdot \text{s}$. The timing resolution for overlapping strips was found to be about 0.7 ns FWHM in bench tests but 1.5–2 ns in the experimental setup. This is possibly due to the ~ 200 ns cable delay between the CFD output and TDC input which is necessary to allow time for the main experiment trigger to generate TDC start signals.

To check the tagger energy resolution with the microscope and to obtain accurate energy calibration the tagger magnetic field was set so that a ~ 0.5 fA electron beam of suitable energy from MAMI passed through the microscope. The beam was scanned across sections of the microscope by varying the magnetic field in the tagger dipole. Each field setting simulates a different electron energy E' given by

$$E' = E \cdot \frac{B}{B'}\,, \tag{1}$$

where E is the electron beam energy, B is the field used in the main tagged-photon experiment and B' is the magnetic field used for each calibration point. Here it is assumed that the shape (see below) of the magnetic field along the electron trajectory does not change as the field is varied.

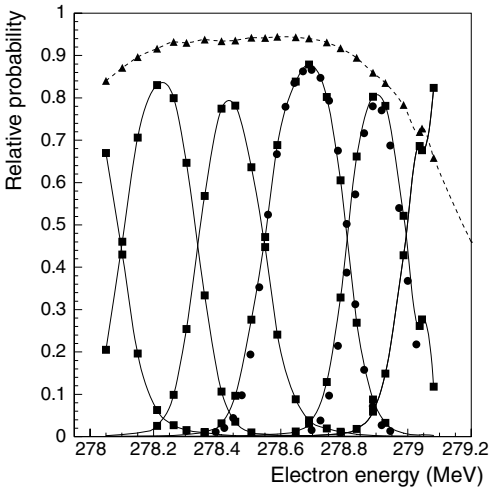

Fig. 5. Relative channel response determined from scanning a 225 MeV calibration electron beam through part of the microscope (squares) and one channel of the main detector array (triangles) by varying the magnetic field slightly around 0.64 T. The microscope was located to cover the tagged-photon energy range from 227 MeV to 268 MeV for an incident electron beam energy of 541 MeV which uses the same field. The lines are drawn to guide the eye and the filled circles show results from a GEANT3 simulation. The tagging electrons cross the focal plane at an angle of about 31.2°.

The typical hit pattern when the calibration beam passes through the microscope is shown in fig. 4. The "tails" above and below the peak arise from scattering in the microscope, in the 1 mm thick aluminium plate which protects the Kapton vacuum window on the tagger exit, and backscattering in the main detector array. The tails are greatly reduced if multiplicity > 2 and non-adjacent multiplicity $= 2$ events are rejected.

The normalised hit pattern for each field setting gives the relative probability that each microscope channel receives a hit for the corresponding simulated (eq. (1)) electron energy. This is shown for a few microscope channels in fig. 5, which also shows results for one of the detectors in the main array obtained in a similar manner. The above procedure simulates the response to different electron energies at constant magnetic field. The conversion from field to electron energy was obtained from ray tracing in an effective uniform field inferred from a field map measured [4] at 1 T. The field map includes the location

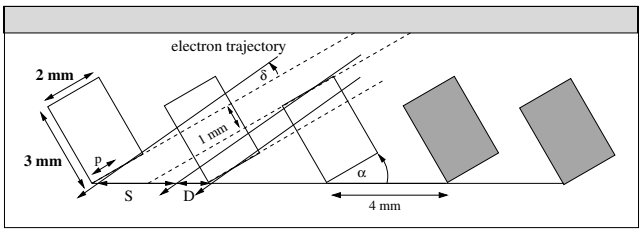

Fig. 6. Geometry of single and double hits at non-normal incidence.

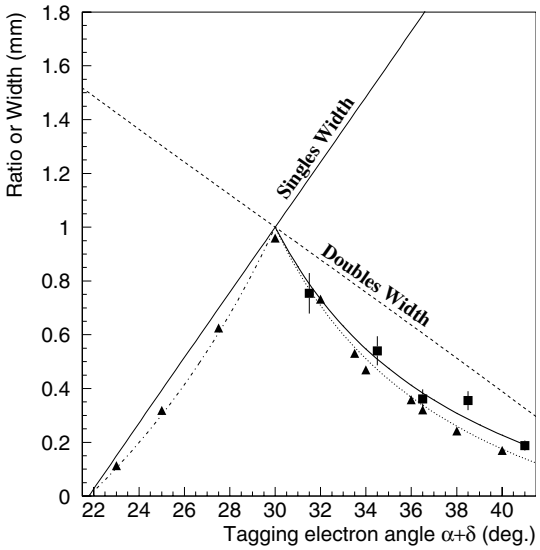

Fig. 7. Projected single- (S, thin solid line) and double- (D, dashed line) hit channel widths and their ratio predicted by eqs. (2)-(4) as a function of the angle $(\alpha + \delta)$ the tagging electron trajectory makes with the focal plane. The width ratio (S/D for angles $< 30^\circ$, D/S for angles $> 30^\circ$) for $p = 1.0\,\mathrm{mm}$ (dot-dashed and dotted lines) and $p = 0.75\,\mathrm{mm}$ (thick solid line) is compared with results from a GEANT3 simulation with $p = 1.0\,\mathrm{mm}$ (triangles) and with the experimentally observed double- to single-hit counts ratio (squares).

of the NMR probe (Scanditronix NMR 751) which provides the measurement of the field. The mapped field is quite uniform between the poles but shows a small stray field outside of the poles. The effective field is constant between the poles, zero outside the poles and the effective field strength is determined by setting $\int B \cdot \mathrm{d}l$ along the path l of the full energy trajectory equal to the corresponding integral from the measured field map. In eq. (1) it is assumed that the stray field simply scales with the field between the poles, *i.e.* the shape of the field along any electron trajectory does not change as the field is varied.

The effect of a range of opening angles associated with the Bremsstrahlung process on the electron resolution in the focal plane was simulated by introducing a Ta foil at the tagger radiator position (see [4]). The $20\,\mathrm{mg/cm^2}$ thickness was chosen to give a similar rms opening angle from multiple scattering. The effect was found to be negligible.

It can be seen (fig. 5) that the resolution is better than that of the main focal-plane detector by a factor of about 6. However, the channel response looks approximately Gaussian, rather than the smeared rectangular response that might be anticipated since the MAMI beam is about 0.1 mm wide and the intrinsic resolution of the spectrometer is $\sim 0.15\,\mathrm{MeV}$ [4]. Simulations using GEANT3 show that this is due to scattering in the 1 mm thick aluminium protection plate which the tagging electrons must pass through before reaching the microscope.

The small difference in spanned energy bite between successive channels evident in fig. 5 is due to the incident electron angle being about 1.2° away from normal incidence on the 3 mm face of the scintillator strips and the consequent difference between the widths of the single- and double-hit channels. From simple geometry (fig. 6) it can be shown that, in the absence of scattering, the double- (D) and single- (S) hit projections (in mm) on to the focal plane are given by

$$\mathrm{D} = 4 - \mathrm{S} \tag{2}$$

and

$$\mathrm{S} = 8 - \frac{3}{\sin(\alpha)} + \frac{A \cdot \tan(\delta)}{[\tan(\alpha) + \tan(\delta)]}\,, \tag{3}$$

where

$$A = \frac{3}{\sin(\alpha)} \mp \frac{2}{\cos(\alpha)} \pm \frac{2p \cdot \cos(\delta)}{\cos(\alpha)}\,. \tag{4}$$

$\alpha = 30^\circ$ is the angle between the normal to the 3 mm wide face of the scintillator strips and the focal plane and $\alpha + \delta$ is the angle which the tagging electron trajectory makes with the focal plane. In eq. (4) the upper (lower) signs apply when δ is greater (less) than zero. In deriving these equations it was assumed that any path traversed through a scintillator strip greater than length p (mm) will lead to an output signal above the discriminator threshold. The projected single- (S) hit and double- (D) hit channel width and the S/D or D/S width ratio from the above equations is plotted as a function of the tagging electron angle $(\alpha+\delta)$ in fig. 7. The D/S ratio from the experimentally observed numbers of single hits and double hits is also plotted. It can be seen that the ratio calculated from the simple formulae agree with a GEANT3 simulation using the same value of p. The experimentally measured ratio agrees better with the simple formulae with $p = 0.75\,\mathrm{mm}$ (which corresponds to an effective threshold in the strips of about $0.14\,\mathrm{MeV}$) rather than $p = 1.0\,\mathrm{mm}$ (which corresponds to a threshold of about $0.18\,\mathrm{MeV}$).

In photon tagging experiments the photon flux is usually based on the counts in scalers connected to each tagger channel. As the scalers in the microscope (see sect. 2) give the counts from the strips rather than the channels, the width ratios are required in order to assign counts between the single- and neighbouring double-hit channels. The fraction of the tagged photons which pass through the tagger collimator and reach the target (the "tagging efficiency", see [5]) can be taken from measurements using the main tagger detector array elements immediately behind the microscope. Alternatively, it can be measured for

each microscope strip or channel provided care is taken to correct for room background —see sect. 2.

When the microscope is located at positions corresponding to tagged-photon energies below about 350 MeV, the channel widths become very unequal and the flux in the very narrow single-hit channels becomes very small, so that the improvement in resolution for most of the photons tagged by the microscope is only a factor of ~ 2. This could be improved by construction of a second microscope where the strips are held at an angle of $\sim 25°$ to the focal plane instead of the present 30°.

4 Tagger energy calibration

The method of ray tracing in an equivalent uniform field is sufficiently accurate (about 1 MeV) to estimate the energy resolution and indeed to calibrate the energy in many tagged-photon experiments, but for more accurate work it is better to make use of the accurately known electron beam energies from the Mainz accelerator. This can produce beam energies in steps of 15 MeV above 180 MeV with an uncertainty of 140 keV (FWHM) [14]. The energy is determined by a precise measurement of the beam position in MAMI as it recirculates round the microtron dipoles which have been precisely field mapped.

The basic calibration at one point on the microscope results from finding the microscope hit position for some calibrating beam energy E. The corresponding tagged-photon energy is $E_e - E$, where E_e is the energy of the incident electron beam used to produce Bremsstrahlung in the main experiment. Different beam energies, E, provide calibration points with an uncertainty equal to that in the difference between E_e and E.

During a calibration run the majority of the counts in the microscope are in one or two channels (fig. 4), so the hit position is taken to be the mean channel. Because of the geometry, selection of multiplicity 1 or 2 events in the microscope removes events where electrons are scattered in the aluminium protection plate and in the microscope.

The 15 MeV energy steps available from MAMI provide only three or four basic calibration points over the range covered by the microscope, but smaller energy steps can be simulated by varying the tagger magnetic field slightly (see sect. 3). To scan across the whole microscope with a single beam energy requires field changes of up to about 30% which results in a significant change in the field shape along the electron trajectory. However, it is possible to quantify this effect by scanning a region of the microscope with one beam of energy such that field values close to B can be used, and then scanning the same region with beam energy higher or lower by 15 MeV (at field B'). The difference between the energy estimated from the microscope hit position and the calibration obtained with field values close to B, and that calculated from eq. (1) gives a correction appropriate for field B'. Corrections for intermediate field values were estimated by assuming that the correction is a linear function of the field.

In a calibration where the microscope covered the photon energy range 673–728 MeV for a main beam energy of 883 MeV, two checks were made on the validity of this procedure. The first was to compare the results of applying it to calibrations using beam energies of 180.12, 195.39 and 210.18 MeV. The resulting overlapping sets of calibration points are shown in fig. 8. The three sets of points were found to be consistent, the rms deviation between two calibrations in the region where they overlapped being less than 0.045 MeV.

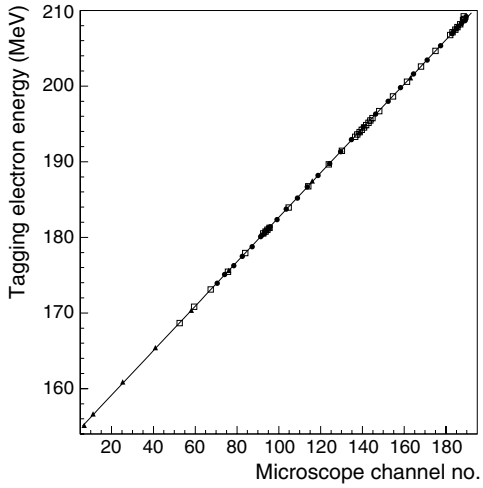

Fig. 8. Microscope energy calibration from scans using electrons of 180.12 (circles), 195.39 (squares) and 210.18 (triangles) MeV after corrections for changes in the shape of the magnetic field in the tagger (see text).

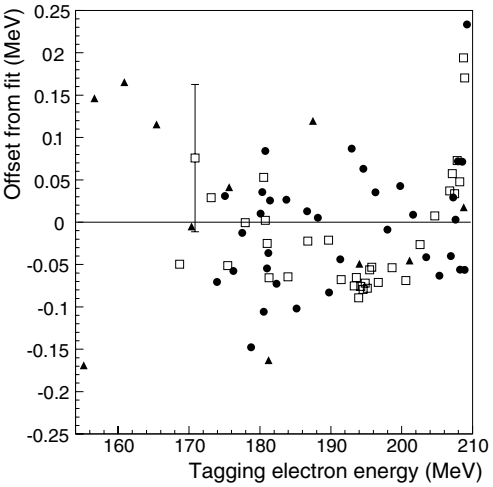

Fig. 9. Deviations of the calibration points from a straight-line fit (symbols as in fig. 8). The error bar indicates the rms deviation.

The second check was to compare the mean calibration from fig. 8 (obtained from a global fit to all the points) with one where all points derived from field changes greater than 4% were omitted. The rms difference between the two calibrations was found to be less than 0.030 MeV.

Deviations of the points from the global fit in fig. 8, shown in fig. 9, give an estimate of the extra uncertainty in regions away from the basic calibration points. In the present example the rms deviation was found to

be 0.087 MeV. Taking the pessimistic view that the uncertainties in all the MAMI beam energies are independent and equal to 0.14 MeV implies the uncertainty in the tagged-photon energy for any microscope channel is $\sqrt{0.14^2 + 0.14^2 + (0.087 \times 2.35)^2} = 0.28$ MeV (FWHM).

As a further check on the reproducibility of the calibration, two more scans were made with MAMI energies close to 180 MeV. By varying the tagger field the simulated tagging electron energies again covered the range 155–210 MeV. In both cases the results were found to be consistent with the calibration shown in fig. 8.

The focal-plane microscope has already been used in several experiments including an attempt to measure the mass of the η-meson by determination of the threshold energy for η photoproduction. The energy calibration shown in fig. 8 is taken from this experiment.

5 Summary

The compact 96-element scintillator array described here improves the energy resolution of the Glasgow photon tagging spectrometer at Mainz by a factor of 2 to 6 over a 60 MeV energy range. It has been shown that by using several accurately known beam energies from the Mainz accelerator it is possible to achieve an energy calibration accuracy of ~ 0.28 MeV FWHM.

We would like to thank Prof. H. Ströher and the technicians at the Institut für Kernphysik, Forschungszentrum Jülich for accurately cutting the 96 scintillator strips. This research was supported by the UK EPSRC, the Deutsche Forschungsgemeinschaft (SFB 443) and DAAD (ARC-program ARC-X-96/21) and is part of the EU integrated infrastructure initiative hadron physics project under contract number RII3-CT-2004-506078.

References

1. T. Teresawa *et al.*, Nucl. Instrum. Methods A **248**, 429 (1986).
2. J.M. Vogt *et al.*, Nucl. Instrum. Methods A **324**, 198 (1993).
3. D.I. Sober *et al.*, Nucl. Instrum. Methods A **440**, 263 (2000).
4. I. Anthony, J.D. Kellie, S.J. Hall, G.J. Miller, Nucl. Instrum. Methods A **301**, 230 (1991).
5. S.J. Hall, G.J. Miller, R. Beck, P. Jennewein, Nucl. Instrum. Methods A **368**, 698 (1996).
6. H. Herminghaus, K.H. Kaiser, H. Euteneuer, Nucl. Instrum. Methods A **138**, 1 (1976).
7. T. Walcher, Prog. Part. Nucl. Phys. **24**, 189 (1990).
8. J. Ahrens *et al.*, Nucl. Phys. News **4**, 5 (1994).
9. D. Lohman *et al.*, Nucl. Instrum. Methods A **343**, 494 (1994).
10. U. Timm, Fortschr. Phys. **17**, 765 (1969).
11. F. Rambo *et al.*, Phys. Rev. C **58**, 489 (1998).
12. K. Livingston, *The Stonehenge Technique: a New Method of Crystal Alignment for Coherent Bremsstrahlung Experiments*, in *International Conference on Charged and Neutral Particle Channeling Phenomena*, edited by Sultan B. Dabagov, Proc. SPIE **5974**, 59740G (2005).
13. B. Krusche *et al.*, Z. Phys. A **351**, 237 (1995).
14. K.-H. Kaiser, private communication; A. Jankoviak *et al.*, Eur. Phys. J. A **28**, s01, 149 (2006) DOI: 10.1140/epja/i2006-09-016-3.